Supporting Information to

Equilibrium mercury isotope fractionation between dissolved Hg(II) species and thiol-bound Hg

Jan G. Wiederhold[1,2], Christopher J. Cramer[3], Kelly Daniel[3], Ivan Infante[4], Bernard Bourdon[2], and Ruben Kretzschmar[1]*

[1] Institute of Biogeochemistry and Pollutant Dynamics, Soil Chemistry, ETH Zurich, Switzerland

[2] Institute of Geochemistry and Petrology, Isotope Geochemistry, ETH Zurich, Switzerland

[3] Department of Chemistry and Supercomputing Institute, University of Minnesota, USA

[4] Department of Physical Chemistry, University of Geneva, Switzerland

* wiederhold@env.ethz.ch, phone: +41-44-6336008, fax: +41-44-6331118

This Supporting Information contains 17 pages, 11 tables, and 7 figures.

content list:

Data tables experimental data:

Samples labeled "C" refer to the Hg(II)-chloride experiments and samples labeled "N" refer to the Hg(II)-nitrate experiments.

Table S1: Experimental results (Hg concentrations and MDF).

			solution	solution	resin-bound	resin-bound	
sample name	dissolved Hg	fraction sorbed	$\delta^{202}Hg_{NIST3133}$	$\delta^{202}Hg_{initial}$	$\delta^{202}Hg_{NIST3133}$	$\delta^{202}Hg_{initial}$	$\varepsilon^{202}Hg_{sol\text{-}resin}$
	[ppm]	[%]	[‰]	[‰]	[‰]	[‰]	[‰]
C0	52.3	0.0	-0.77	0.00	-	-	-
C1	51.4	1.8	-0.71	0.07	-1.31	-0.53	0.60
C4	41.9	19.9	-0.71	0.07	-1.23	-0.46	0.53
C6	32.5	37.8	-0.65	0.13	-1.06	-0.28	0.41
C7	24.1	54.0	-0.50	0.28	-0.98	-0.21	0.49
C9	9.3	82.2	-0.28	0.50	-0.86	-0.09	0.58
C10	1.1	98.0	-0.17	0.60	-0.77	0.00	0.60
						average:	0.53
						2SD	0.15
N0	71.3	0.0	-0.54	0.00	-	-	-
N1	71.1	0.2	-0.41	0.13	-1.03	-0.49	0.62
N4	57.7	19.1	-0.49	0.05	-0.95	-0.42	0.47
N7	44.9	37.1	-0.16	0.38	-0.85	-0.31	0.69
N8	33.4	53.2	-0.15	0.39	-0.75	-0.21	0.61
N9	22.6	68.4	0.00	0.54	-0.71	-0.17	0.71
N10	13.0	81.8	0.01	0.55	-0.61	-0.07	0.62
						average:	0.62
						2SD	0.17

Table S2: MIF in experimental data for odd Hg isotopes ($\Delta^{199}Hg$ and $\Delta^{201}Hg$).

	solution	solution	solution	solution	resin-bound	resin-bound	resin-bound	resin-bound
sample name	$\Delta^{199}Hg$ NIST3133 [‰]	$\Delta^{199}Hg$ initial [‰]	$\Delta^{201}Hg$ NIST3133 [‰]	$\Delta^{201}Hg$ initial [‰]	$\Delta^{199}Hg$ NIST3133 [‰]	$\Delta^{199}Hg$ initial [‰]	$\Delta^{201}Hg$ NIST3133 [‰]	$\Delta^{201}Hg$ initial [‰]
C0	0.010	0.000	-0.009	0.000	-	-	-	-
C1	0.035	0.025	-0.007	0.002	0.041	0.031	0.003	0.013
C4	0.010	0.000	-0.016	-0.006	0.047	0.037	0.014	0.024
C6	0.010	0.000	-0.016	-0.007	0.011	0.001	-0.006	0.003
C7	0.003	-0.007	-0.018	-0.008	0.017	0.007	-0.015	-0.006
C9	-0.010	-0.020	-0.015	-0.005	0.008	-0.002	-0.006	0.003
C10	-0.015	-0.025	-0.024	-0.014	0.015	0.005	-0.011	-0.002
N0	-0.015	0.000	-0.028	0.000	-	-	-	-
N1	-0.009	0.006	-0.035	-0.007	0.052	0.067	0.015	0.044
N4	-0.004	0.011	-0.031	-0.003	0.034	0.049	0.002	0.030
N7	-0.020	-0.005	-0.029	-0.001	0.044	0.059	-0.021	0.007
N8	-0.043	-0.028	-0.068	-0.040	0.000	0.015	-0.005	0.023
N9	-0.030	-0.015	-0.056	-0.028	-0.008	0.006	-0.006	0.022
N10	-0.052	-0.037	-0.060	-0.032	0.015	0.030	-0.033	-0.005

Table S3: MIF in experimental data for even Hg isotopes (Δ^{200}Hg and Δ^{204}Hg).

sample name	solution Δ^{200}Hg NIST3133 [‰]	solution Δ^{200}Hg initial [‰]	solution Δ^{204}Hg NIST3133 [‰]	solution Δ^{204}Hg initial [‰]	resin-bound Δ^{200}Hg NIST3133 [‰]	resin-bound Δ^{200}Hg initial [‰]	resin-bound Δ^{204}Hg NIST3133 [‰]	resin-bound Δ^{204}Hg initial [‰]
C0	0.009	0.000	-0.024	0.000	-	-	-	-
C1	0.020	0.011	-0.023	0.001	0.015	0.006	0.026	0.050
C4	-0.001	-0.010	-0.023	0.001	0.023	0.014	-0.017	0.007
C6	0.012	0.003	-0.028	-0.004	0.003	-0.006	0.000	0.024
C7	0.006	-0.002	-0.020	0.004	-0.003	-0.011	-0.008	0.015
C9	0.011	0.002	-0.016	0.007	0.009	0.000	0.012	0.036
C10	0.003	-0.006	0.006	0.030	0.016	0.008	0.003	0.026
N0	0.001	0.000	0.031	0.000	-	-	-	-
N1	0.011	0.010	0.002	-0.029	0.011	0.010	-0.002	-0.033
N4	0.005	0.004	-0.001	-0.032	0.013	0.012	0.004	-0.027
N7	0.001	0.000	0.028	-0.003	-0.003	-0.004	-0.024	-0.055
N8	-0.017	-0.018	-0.042	-0.074	-0.002	-0.003	0.024	-0.007
N9	0.022	0.021	0.015	-0.016	0.028	0.027	0.001	-0.030
N10	-0.012	-0.013	-0.017	-0.048	0.018	0.016	0.010	-0.022

Table S4: Wilcoxon signed-rank test for difference between "solution" and "resin-bound" samples

	Δ^{199}Hg	Δ^{201}Hg	Δ^{200}Hg	Δ^{204}Hg
p-value	0.0005	0.0005	0.2661	0.1514
(pseudo)median of difference	-0.033	-0.024	-0.005	-0.012
lower limit 95% confidence interval	-0.049	-0.038	-0.014	-0.031
upper limit 95% confidence interval	-0.018	-0.010	0.004	0.004

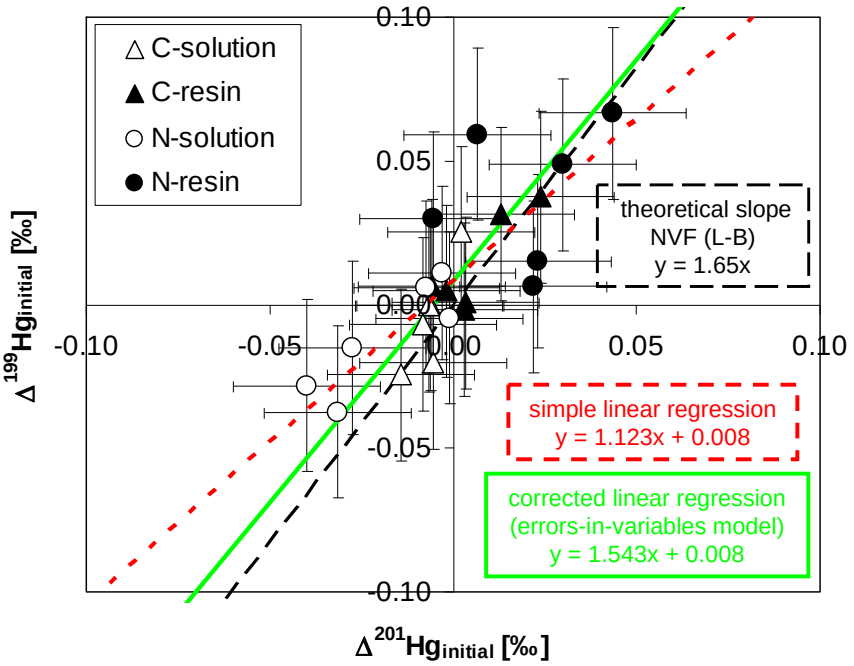

Figure S1: Comparison of linear regression methods for data presented in Figure 6. The simple linear regression method (dashed red line) neglects the uncertainty in x-direction and results in a significant underestimation of the slope. The corrected linear regression (solid green line) considers the uncertainty in both dimensions (errors-in-variables model[1]) resulting in a slope which is much closer to the theory.

[1] see e.g., Fuller, W.A. *Measurement Error Models*. John Wiley & Sons, New York, 1987.

Data table computational data:

Table S5: Calculated 1000 ln β values at 298.15 K relative to elemental Hg vapor for different Hg isotope ratios and separated into the contributions by nuclear volume fractionation (NVF) and mass-dependent fractionation (MDF).

	$Hg(SMe)^+$	$Hg(SH)^+$	$Hg(SMe)_2$	$Hg(SH)_2$	HgSMeOH	HgSHCl	$HgOH^+$	HgSHOH	$HgCl^+$	HgSMeCl	$HgCl_2$	HgClOH	$Hg(OH)_2$	$HgCl_4^{2-}$
202/198														
sum	1.04	1.28	1.53	1.63	1.90	1.80	1.82	1.88	1.88	1.78	2.09	2.17	2.19	2.63
NVF	0.79	0.97	0.82	0.91	0.90	1.04	1.41	0.96	1.49	0.98	1.25	1.11	1.00	2.23
MDF	0.26	0.31	0.70	0.73	1.00	0.76	0.42	0.92	0.39	0.80	0.84	1.06	1.19	0.40
202/199														
sum	0.93	1.15	1.31	1.40	1.60	1.55	1.64	1.59	1.70	1.52	1.81	1.84	1.84	2.41
NVF	0.74	0.92	0.78	0.86	0.85	0.98	1.33	0.91	1.41	0.92	1.18	1.05	0.95	2.11
MDF	0.19	0.23	0.53	0.54	0.75	0.57	0.31	0.69	0.29	0.60	0.63	0.79	0.89	0.30
202/200														
sum	0.54	0.67	0.78	0.84	0.97	0.92	0.95	0.96	0.98	0.91	1.07	1.11	1.12	1.37
NVF	0.41	0.51	0.43	0.48	0.47	0.55	0.74	0.50	0.79	0.51	0.66	0.59	0.53	1.17
MDF	0.13	0.15	0.35	0.36	0.49	0.38	0.21	0.46	0.19	0.40	0.41	0.52	0.59	0.20
202/201														
sum	0.35	0.44	0.48	0.51	0.58	0.57	0.62	0.58	0.64	0.56	0.67	0.67	0.66	0.92
NVF	0.29	0.36	0.30	0.33	0.33	0.38	0.52	0.35	0.55	0.36	0.46	0.41	0.37	0.82
MDF	0.06	0.08	0.17	0.18	0.25	0.19	0.10	0.23	0.10	0.20	0.21	0.26	0.29	0.10
202/204														
sum	-0.58	-0.71	-0.82	-0.87	-1.01	-0.97	-1.01	-1.00	-1.05	-0.95	-1.13	-1.15	-1.15	-1.48
NVF	-0.45	-0.56	-0.48	-0.52	-0.52	-0.60	-0.81	-0.55	-0.86	-0.56	-0.72	-0.64	-0.58	-1.29
MDF	-0.12	-0.15	-0.34	-0.35	-0.49	-0.37	-0.20	-0.45	-0.19	-0.39	-0.41	-0.51	-0.58	-0.19
202/196														
sum	1.50	1.85	2.24	2.39	2.79	2.62	2.63	2.75	2.70	2.60	3.04	3.18	3.22	3.77
NVF	1.12	1.38	1.17	1.29	1.28	1.48	2.00	1.36	2.12	1.39	1.78	1.58	1.42	3.17
MDF	0.39	0.47	1.07	1.10	1.51	1.15	0.63	1.39	0.58	1.22	1.27	1.60	1.81	0.61

Temperature dependence of computational data:

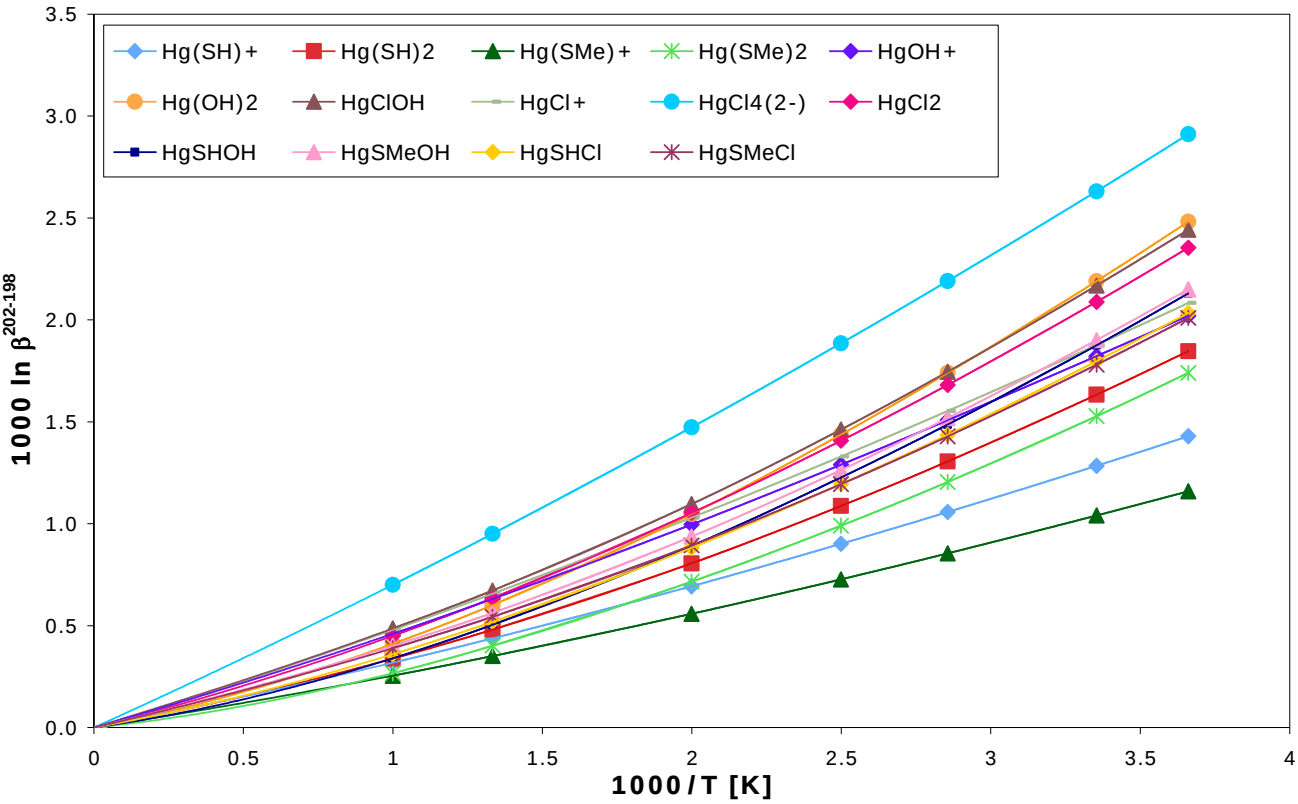

Figure S2: Temperature dependence of calculated 1000 ln $\beta^{202-198}$ values caused by the combination of mass-dependent (MDF) and nuclear volume fractionation (NVF). MDF scales as $1/T^2$ whereas NVF scales as 1/T, which results in a higher relative contribution of NVF at higher temperatures.

Supporting information to the analytical methods:

In the following section, some additional analytical details of the Hg isotope ratio measurement by cold vapor MC-ICPMS (Cetac HGX-200 coupled to Nu Plasma) are described. The quantitative reduction of Hg(II) from sample solutions to Hg^0 after mixing with $Sn(II)Cl_2$ and removal in the gas-liquid separator (frosted glass post design) was tested by collecting the waste solution of the HGX-200 after several minutes of uptake of a 20 μg L^{-1} Hg solution (1% BrCl matrix) in concentrated BrCl solution and analyzing the Hg concentration by CV-AFS. The obtained Hg concentration value of 0.04 μg L^{-1} Hg was indistinguishable from the Hg concentration measured for the concentrated BrCl solution used for trapping the HGX-200 waste solution, indicating a quantitative Hg removal from the sample solutions. The mass bias correction with Tl was performed by assuming an exponential fractionation law and using a $^{205}Tl/^{203}Tl$ ratio of 2.38714 in NIST-997. The Tl corrected ratios were then in a second step reported relative to the Tl corrected Hg isotope ratios of the average of the previous and following NIST-3133 solutions (sample-standard bracketing). Washout in-between samples was performed by a sequence of 5% BrCl solution (3 min) and 1% BrCl solution (usually 5 min) for Hg and 0.1M HNO_3 for Tl (introduced through Aridus desolvating nebulizer) until the intensities of all masses reached background levels. On-peak zero measurements (60 s integration time) of all collected masses were performed before each sample measurement and used for background correction. The sample analysis consisted of one cycle with 36 measurements (5 s integration time each) collecting intensities on masses 194, 196, 198, 199, 200, 201, 202, 203, 204, 205, 206, and 208. The beams collected on masses 194, 206, and 208 were always at background level, indicating that potential Pt interferences on mass 196 and 198 and Pb interferences on mass 204 were negligible. The setup of the collector block is depicted in Table S6.

Table S6: Collector setup of Nu Plasma MC-ICPMS used for Hg isotope ratio analysis

cup	H6	X	H5	H4	H3	H2	H1	Ax	L1	L2	L3	X	L4	IC0	L5
mass	208		206	205	204	203	202	201	200	199	198		196		194
Hg					Hg		Hg	Hg	Hg	Hg	Hg		Hg		
other	Pb		Pb	Tl	Pb	Tl					Pt		Pt		Pt

Supporting information to the computational methods:

(additional references are cited in squared brackets and listed at the end of this section)

In order to compute the Nuclear Volume Fractionation (NVF), a quantum chemistry program that describes the nucleus as having a finite volume (and not as a point charge, as is done in most non-relativistic software packages) is required. In relativistic theory, it is known that the use of a point-charge model introduces artifacts in the radial solution of the Dirac equation [1]. To overcome this problem, the 4-component DIRAC08 code [2] employs a computationally favorable finite nucleus model [3], based on a Gaussian distribution function, which is physically sound as an approximation to the nuclear charge distribution. The DIRAC08 program had additional advantages for our purposes, including a) the inclusion of relativistic effects and spin-orbit coupling from the outset, so that mixing of orbitals with different orbital angular momenta is included already at the Hartree-Fock (HF) level; b) the description of the electronic core is done through solution of the 4-component Dirac equation, so that the core electron density is described explicitly and not through pseudopotentials (PP); c) the availability of accurate single-reference methods to describe the ground state of the atoms and molecules studied here (e.g., DC-MP2, DC-CCSD, and DC-CCSD(T)). In the 4-component framework, the two-electron interaction is generally described by a simple columbic term plus a retardation effect called Breit interaction. This latter contribution is usually very small for chemical purposes and is normally neglected. The two-electron interaction used includes only the Coulomb term, hence the acronym DC, which stands for Dirac-Coulomb.

In all the post-HF calculations, the computed correlation energy depends on the choice of the active space that consists of the 5d and 6s orbitals of mercury (12 electrons in total), the 1s for hydrogen (1 electron), the 2s and 2p for oxygen and carbon (6 and 4 electrons, respectively), the 3s and 3p for sulfur and chlorine (6 and 7 electrons). We also reduced the full set of virtual orbitals to those relevant for valence and subvalence correlation; we did so by deleting virtuals with an orbital energy above 10 a.u.

For purpose of analysis we have also made use of the transformed DC equation, which can be approximated to the scalar relativistic spin-free (SFDC) Hamiltonian [4] or to the non-relativistic solution (i.e., Levy-Leblond) [5]. For computational efficiency only the (LL|LL) and (SS|LL) two-electron integrals (L=large; S=small) were included. Test calculations that included the more numerous but numerically insignificant (SS|SS) integrals showed that associated error is marginal. The Dyall uncontracted double-zeta basis for the Hg atom of 22s19p12d8f size has been used [6]. Tests calculations (vide infra) have been carried out using a larger triple-zeta basis set of 29s24p15d10f1g size. For the lighter elements H, O, C, S, Cl, we made use of the cc-pVDZ or cc-pVTZ basis sets of Dunning and Woon [7–8].

As also described by Schauble [9], in DIRAC08 the radial charge density is approximated by a single Gaussian function, whose exponent is directly related to the radius of the nucleus of a given isotope (Table S7). The NVF has been computed for several isotopes of Hg: ^{196}Hg, ^{198}Hg, ^{199}Hg, ^{200}Hg, ^{201}Hg and ^{204}Hg. The following formula has been used:

$$1000 \cdot ln\beta_{202-Y}^{NV} = 10^3 \frac{\left(E\left[^{202}\mathrm{Hg}^0\right] - E\left[^{Y}\mathrm{Hg}^0\right]\right) - \left(E\left[^{202}\mathrm{HgX}^0\right] - E\left[^{Y}\mathrm{HgX}^0\right]\right)}{kT} \quad (1)$$

All of the isotopes have been compared to the most aboundant ^{202}Hg isotope.

Table S7: Values of the Gaussian exponent ξ used to approximate the radial charge-density of each isotopic nucleus as measured using the Landolt-Boernstein radii *(38)*. All ξ values are expressed in atomic units and the root mean squared (rms) charge radius in fm.

$\xi = 3/[2\langle r^2_{NUC}\rangle]$		
	$\langle r^2_{NUC}\rangle^{1/2}$	ξ
196	5.435	1.421981944E+08
198	5.443	1.417805021E+08
199	5.444	1.417284200E+08
200	5.452	1.413127944E+08
201	5.455	1.411574060E+08
202	5.462	1.407958283E+08
204	5.472	1.402816939E+08

As previously explained [9], electrons with higher probability to be found at the nucleus, such as the *s* electrons, are more strongly bound to small sized isotopes, while electrons with higher angular momenta are stabilized around larger isotopes. Hence, a larger or smaller stabilization of the electrons around the nuclei is an electronic effect and depends on the reciprocal screening between electrons of different angular momenta, which means also from electrons more likely lying far from the nucleus. The NVF is thus implicitly dependent on the total electron density and not only on the core electron density.

In Fig. S3 we have depicted the NVF of $HgCl_2$ as a function of 1000/T for several computational methods. Taking the DC-CCSD(T)/TZ as the reference value, it is soon clear that the less accurate approach, DHF, tend to overestimate the NVF, even though it keeps a correct qualitative trend. All the other post-HF approaches have roughly similar values independently of the basis set chosen. For all the molecules chosen for this paper, we finally decided to use the MP2/DZ method because it gives the closest results to the reference DC-CCSD(T)/TZ values and is much cheaper from a computational standpoint.

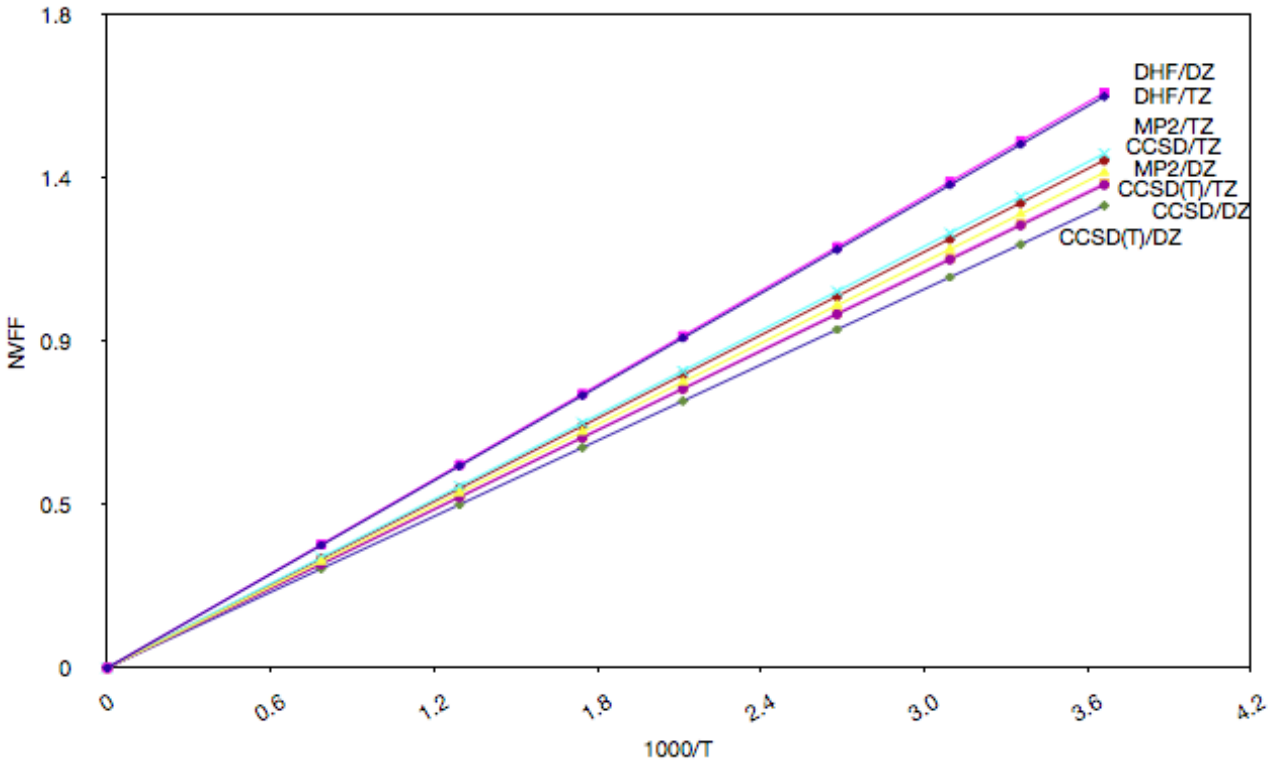

Figure S3: Nuclear volume fractionation factors computed as a function of 1000/T at different level of theories for the $HgCl_2$ molecule. The reference system is vaporous Hg atom, while the isotopes are the most abundant ^{202}Hg and the ^{198}Hg.

From the literature [10], it is known that the heavier elements show a NVF much larger than lighter elements and this has been demonstrated also from first principles by Schauble [9]. However, up to now it is not yet known what is the driving force that enhances this fractionation for heavy elements.

We decided to carry out calculations in which, starting from the full 4-component solution of the Dirac equation, we "switch off" the spin-orbit coupling term (SF-DC-MP2 = Spin-Free-DC-MP2) [4] and the relativistic effects (NR-MP2 = Non Relativistic MP2) [5] at same basis set level of theory. In Fig. S4, we have depicted the NVF of $HgCl_2$ as a function of 1000/T for all the three type of approximations. It is soon clear that the NR solution gives much smaller nuclear volume fractionations, indication a trend more in line with the lighter elements, where usually such type of fractionation is negligible as compared to the mass-dependent one.

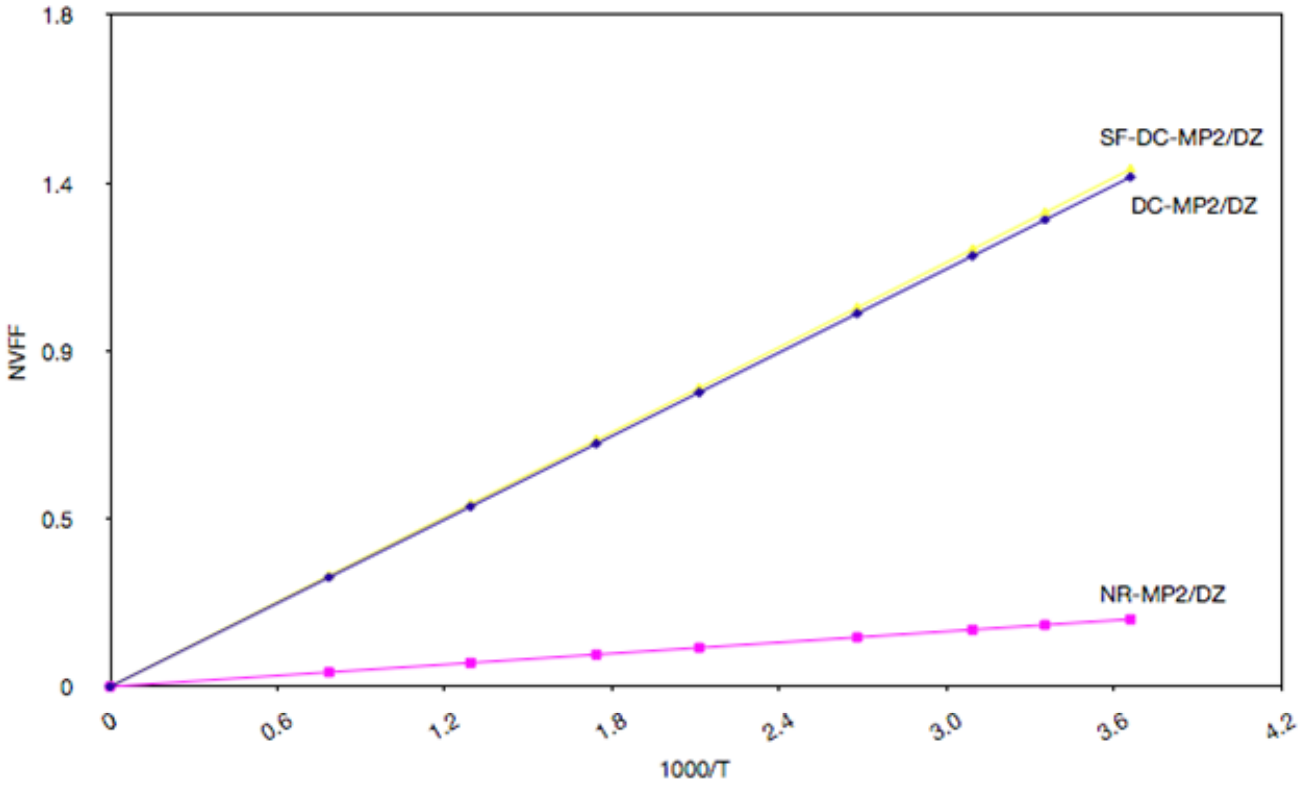

Figure S4: Nuclear volume fractionation factors computed as a function of 1000/T at MP2 level of theory for the $HgCl_2$ molecule. The reference system is vaporous Hg atom, while the isotopes are the most abundant ^{202}Hg and the ^{198}Hg. Three level of approximations have been considered: the full 4-component solution, the transformed Spin-Free Dyall's solution and the non-relativistic Levy-Leblond transformation.

From formula (1), we can think the NVF as a difference of difference of energies, ΔΔE, in which the first ΔE represents the isotopic total energy change for a given species, and the second ΔΔE is the energy differential between the ΔE's of two different type of molecules. By looking at Table S8, we immediately notice how that the magnitude of the ΔE for vaporous Hg for both the full DC-MP2 and the SF-DC-MP2 method is approximately six times larger than the non relativistic value. This large gap is evenly present also in the $HgCl_2$ molecule. This large damping in the total energy difference between two isotopes in a non-relativistic framework brings to a damping also in the ΔΔE values as a consequence, yielding a smaller fractionation.

Table S8: Total energy difference (a.u.) between two different isotopes of a given species.

$E[^{202}Hg^0]- E[^{198}Hg^0]$			$E[^{202}HgCl_2]- E[^{198}HgCl_2]$		
4-comp	Spin-Free	Non-Rel	4-comp	Spin-Free	Non-Rel
0.02638833	0.02618744	0.00445780	0.02638715	0.02618624	0.00445765

A possible qualitative explanation of why relativistic effects have such large impact in the NVF may be appointed to the fact that in heavy atoms the electrons closer to the nuclei move at speed closer to the speed of light. At these velocities, the radial distributions of the *s* and *p* type of orbitals suffer a contraction and the *d* and *f* shells are more diffuse due to a larger screening of the inner electrons. As a consequence, the magnitude of the difference between two isotopes is enhanced since higher electron densities at the nucleus region favors smaller isotopes, as we have seen in the previous section. This in turns gives a larger NVF, which can be identified as a relativistic consequence.

For the non-relativistic DFT calculations, MN-GFM [11], a locally modified version of the Gaussian03 program [12], was employed. In terms of theoretical protocol, we elected to employ gas-phase structures computed at the M06-L level of density functional theory as our source for geometries and molecular partition functions. A reviewer enquired about the "error" associated with the calculations. As a matter of statistical precision, there is no error whatsoever in the calculations. That is, repeating the calculation will always give the identical answer. On the other hand, there is the legitimate

question of, “how does the chosen modeling protocol potentially include errors?” There is, however, no easy answer to this question. One could, in principle, carry out calculations with many different density functionals, but it is not true that an average over functionals will necessarily lead to a more accurate result than any single functional. One can attempt to calibrate DFT predictions against experimental structural and vibrational data, but data are sparse for many of these compounds and their direct correlation with predicted isotope fractionation is not obvious in any case. In terms of the choice of functional, we consider M06-L to have been demonstrated to be well suited for calculations involving metals [13] and we chose it accordingly.

Another modeling choice open to question is the employ of gas-phase calculations as opposed to calculations that attempt to include the effects of aqueous solvation. Solvation effects, however, are not trivial to include and can lead to certain technical complications. A popular approach to include solvation is to employ a continuum solvation model, and geometries optimized under continuum solvation would be expected to more closely conform to those found in actual solution. However, it is not true that vibrational frequencies computed for such geometries should necessarily be better than gas-phase frequencies. A continuum model implicitly assumes full equilibrium between the surrounding solvent and the solute, but vibrational motion occurs on a time scale similar to solvent orientational motions, and as such molecular vibrations in solution are non-equilibrium in nature. Moreover, most modern continuum models require numerical estimation of certain integrals associated with solvation free energies, and noise associated with numerical quadrature can swamp changes associated with heavy-atom isotopes. Given these complications, we decided not to use continuum solvent models. Of course, one could in principle attempt to include explicit solvent, but such calculations require extensive samplings over the phase space of supermolecular conformations, and moreover lead to systems so large that relativistic calculations are impractical.

Thus, there is certainly some reason to suspect that good results between computed and measured values in this work may result in part from a cancellation of errors associated with various approximations in the modeling protocol, but that is, in some sense, an unavoidable consequence of

employing quantum chemical theory to make predictions. Finally, for another discourse of this topic, we refer to the detailed discussion on model accuracy and uncertainty in MDF and NVF calculations in the appendix of the previous publication of Schauble (2007) [9].

[1] Boys, SF, Proc. Roy. Soc. A, **200**, 542 (1950).

[2] DIRAC, a relativistic ab initio electronic structure program, Release DIRAC08 (2008), written by L. Visscher, H. J. Aa. Jensen, and T. Saue, with new contributions from R. Bast, S. Dubillard, K. G. Dyall, U. Ekström, E. Eliav, T. Fleig, A. S. P. Gomes, T. U. Helgaker, J. Henriksson, M. Iliaš, Ch. R. Jacob, S. Knecht, P. Norman, J. Olsen, M. Pernpointner, K. Ruud, P. Sałek, and J. Sikkema (see http://dirac.chem.sdu.dk).

[3] Visser, O. Aerts, OJC Hegarty, D and Nieuwpoort, WC, Chem Phys. Lett., **134**, 34 (1987).

[4] K. G. Dyall, J. Chem. Phys. **100**, 2118 (1994).

[5] Levy-Leblond, JM, Commun. Math. Phys., **6**, 286 (1967).

[6] Dyall KG, Theor. Chem. Acc. **112,** 403 (2004).

[7] T.H. Dunning, Jr. J. Chem. Phys. **90**, 1007 (1989). [for Carbon, Oxygen, Hydrogen];

[8] D.E. Woon and T.H. Dunning, Jr. J. Chem. Phys. **98**, 1358 (1993). [for Sulfur and Chlorine]

[9] Schauble, EA, Geochimica et Cosmochimica Acta, **71**, 2170 (2007).

[10] Knyazev, DA and Myasoedov, NF, Sep. Sci. Technol., **36**, 1677 (2001).

[11] Zhao, Y.; Truhlar, D. G. *MN-GFM version 4.1*; University of Minnesota: Minneapolis, 2008.

[12] Frisch, M. J.; Trucks, G. W.; Schlegel, H. B.; Scuseria, G. E.; Robb, M. A.; Cheeseman, J. R.; Montgomery, J. A.; Vreven, T.; Kudin, K. N.; Burant, J. C.; Millam, J. M.; Iyengar, S. S.; Tomasi, J.; Barone, V.; Mennucci, B.; Cossi, M.; Scalmani, G.; Rega, N.; Petersson, G. A.; Nakatsuji, H.; Hada, M.; Ehara, M.; Toyota, K.; Fukuda, R.; Hasegawa, J.; Ishida, M.; Nakajima, T.; Honda, Y.; Kitao, O.; Nakai, H.; Klene, M.; Li, X.; Knox, J. E.; Hratchian, H. P.; Cross, J. B.; Adamo, C.; Jaramillo, J.; Gomperts, R.; Stratmann, R. E.; Yazyev, O.; Austin, A. J.; Cammi, R.; Pomelli, C.; Ochterski, J. W.; Ayala, P. Y.; Morokuma, K.; Voth, G. A.; Salvador, P.; Dannenberg, J. J.; Zakrzewski, V. G.; Dapprich, S.; Daniels, A. D.; Strain, M. C.; Farkas, O.; Malick, D. K.; Rabuck, A. D.; Raghavachari, K.; Foresman, J. B.; Ortiz, J. V.; Cui, Q.; Baboul, A. G.; Clifford, S.; Cioslowski, J.; Stefanov, B. B.; Liu, G.; Liashenko, A.; Piskorz, P.; Komaromi, I.; Martin, R. L.; Fox, D. J.; Keith, T.; Al-Laham, M. A.; Peng, C. Y.; Nanayakkara, A.; Challacombe, M.; Gill, P. M. W.; Johnson, B.; Chen, W.; Wong, M. W.; Gonzalez, C.; Pople, J. A. *Gaussian 03, Revision D.01*; Gaussian, Inc.: Wallingford, CT, 2004.

[13] Cramer, C. J.; Truhlar, D. G. Density Functional Theory for Transition Metals and Transition Metal Chemistry. Phys. Chem. Chem. Phys. **11**, 10757-10816 (2009).

Table S9: Compilation of calculated (M06-L) q values and structural and vibrational data:

	$Hg(SMe)^+$	$Hg(SMe)_2$	Hg(SMe)OH	$Hg(SH)_2$	Hg(SH)OH	$Hg(SH)^+$	Hg(SMe)Cl	$Hg(OH)_2$	Hg(SH)Cl	Hg(OH)Cl	$HgCl_2$	$Hg(OH)^+$	$HgCl^+$	$HgCl_4^{2-}$
q_{Hg} (a.u.)	0.621	0.678	0.751	0.735	0.773	0.788	0.841	0.84	0.863	0.922	1.005	1.107	1.056	1.657
r_{HgS} (Å)	2.357	2.347	2.317	2.348	2.317	2.324	2.322	-	2.320	-	-	-	-	-
r_{HgO} (Å)	-	-	2.009	-	2.004	-	-	1.984	-	1.988	-	1.994	-	-
r_{HgCl} (Å)	-	-	-	-	-	-	2.311	-	2.301	2.275	2.274	-	2.248	2.602
Vibrational frequencies (cm^{-1})	161.3 199.4 313.7 695.2 911.3 975.5 1320.7 1378.3 1447.8 3001.9 3115.1 3185.2	36.8 70.6 71.7 130.6 131.4 170.2 179.9 315.9 361.8 713.2 714.1 965.0 966.1 968.2 968.6 1345.2 1346.9 1467.4 1467.5 1476.0 1476.2 3044.4 3044.7 3147.4 3147.5 3148.0 3148.0	100.5 121.0 151.0 167.2 194.5 354.4 561.3 713.8 915.2 967.0 971.0 1346.9 1467.2 1474.8 3045.9 3149.7 3150.6 3869.0	93.2 94.7 103.4 318.5 359.8 688.0 726.2 2735.9 2737.1	131.7 132.1 159.8 354.4 569.6 707.3 924.7 2728.9 3868.2	335.5 746.9 2696.1	73.6 90.3 145.0 179.8 323.6 374.4 711.4 967.0 970.7 1347.8 1465.0 1474.9 3047.9 3152.3 3155.6	149.5 177.4 186.4 548.2 624.5 954.3 963.8 3866.7 3868.3	94.9 97.1 327.9 377.4 718.4 2739.0	132.9 140.7 360.9 586.8 962.7 3860.6	99.6 341.2 393.4	536.3 1035.4 3716.3	374.3	48.8 70.9 190.0 220.8

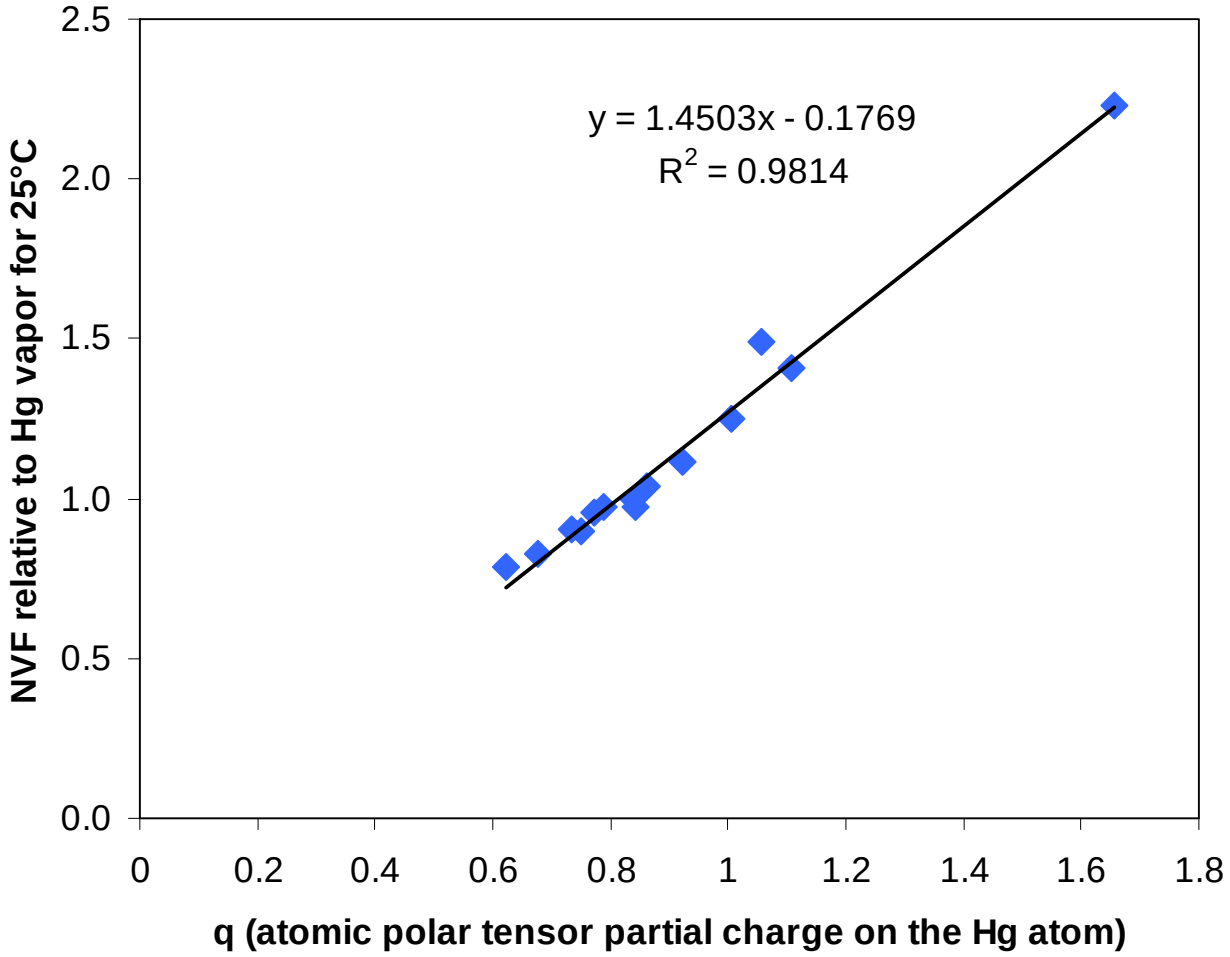

Figure S5: Relationship between calculated values for NVF relative to Hg vapor (for 25°C) and q (atomic polar tensor partial charge on the Hg atom) for the 14 Hg species investigated in this study. The empirical correlation could be useful to estimate NVF for other Hg species (NVF = 1.4503 × q – 0.1769) without the need of relativistic calculations.

Comparison of computational results of Schauble (2007, GCA, *39*) and this study

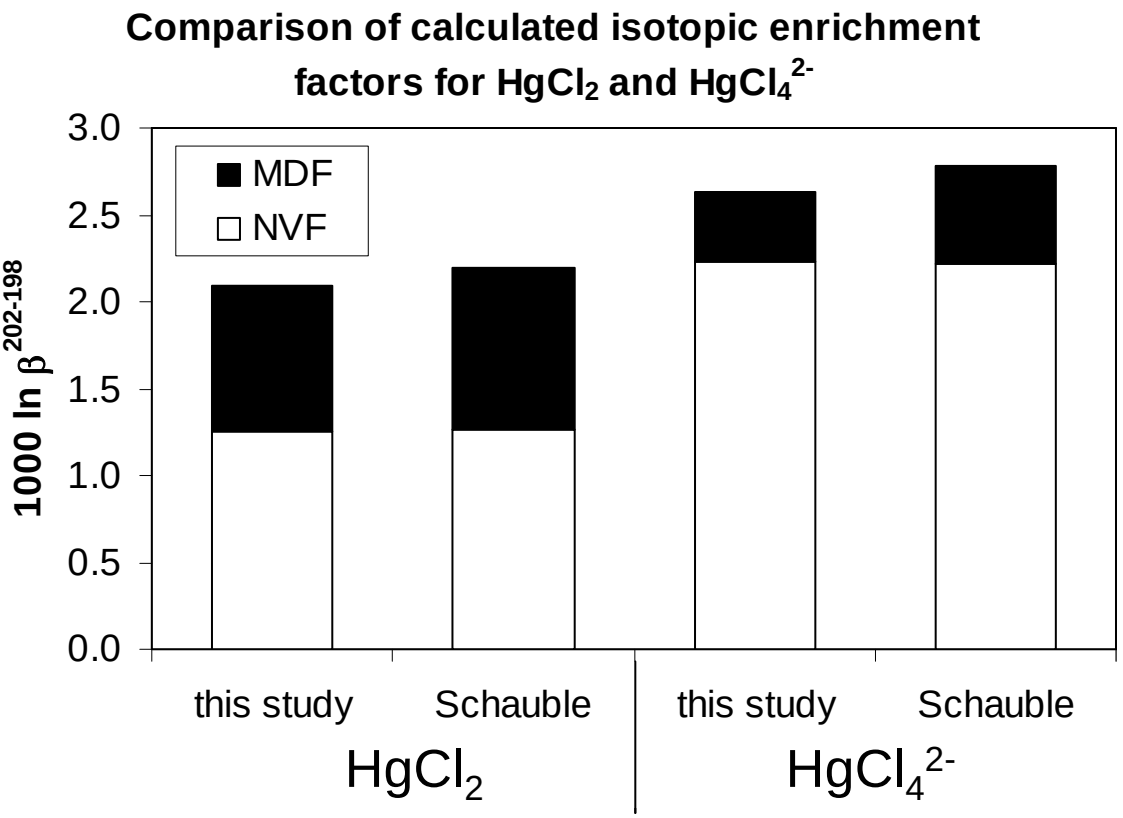

Figure S6: Comparison of computational results for $HgCl_2$ and $HgCl_4^{2-}$ (fractionations relative to Hg vapor at 25°C) reported by Schauble *(39)* and obtained in this study.

In addition, we carried out the necessary DFT calculations to obtain q values for compounds studied by Schauble *(39)* and based on computed APT charges and the linear correlation (NVF = 1.4503 × q – 0.1769) we predicted NVF values of 1.05, 0.98, and 0.75 for $HgBr_2$, HgMeCl, and $HgMe_2$, respectively. These may be compared with Schauble's relativistically computed values of 1.23, 0.80, and 0.57, respectively. The mean unsigned error of 0.18 over these three compounds compares to a mean unsigned error over the compounds in Fig. S5 of 0.04. The larger error may be associated with the Schauble relativistic calculations having been done at the Dirac-Hartree-Fock level, as opposed to the MP2 level employed here (which includes dynamical electron correlation; see previous section in SI), but we have not investigated this point in additional detail.

Comparison of nuclear charge radii and scaling factors for Hg isotopes

Table S10: Comparison of nuclear charge radii for Hg isotopes reported in *(38)* and *(49)*

	mass	196	198	199	200	201	202	204
Landolt-Boernstein[1]	R [fm]	**5.435**	**5.443**	**5.444**	**5.452**	**5.455**	**5.462**	**5.472**
Angeli[2]	R [fm]	**5.4388**	**5.4466**	**5.4484**	**5.4549**	**5.4583**	**5.4633**	**5.4742**

[1] used in this study
[2] used in Schauble *(39)*

Table S11: Comparison of scaling factors for Hg isotope ratios relative to 202/198

	196/198	**199/198**	**200/198**	**201/198**	**202/198**	**204/198**
Mass-dependent kinetic	-0.5074	0.2520	0.5024	0.7520	1	1.4928
Mass-dependent equilibrium	-0.5151	0.2539	0.5049	0.7539	1	1.4855
Nuclear volume (Landolt-Boernstein)	-0.4200	0.0525	0.4732	0.6312	1	1.5277
Nuclear volume (Angeli)[1]	-0.4660	0.1076	0.4966	0.7003	1	1.6543
Nuclear volume (Hahn et al.)[2]	n.d.	0.0804	0.4712	0.6838	1	1.4994

[1] used in Schauble *(39)*
[2] values adopted from Estrade et al. *(16)*

In principle, we could have used the equilibrium mass-dependent fractionation factors to calculate the measured and modeled MIF in our system. However, the difference would not be apparent at the level of significant digits with which we report our results. Moreover, it could be potentially confusing if different scaling factors would be used to calculate Δ^{199}Hg and Δ^{201}Hg values in different studies. The nomenclature proposed by Blum&Bergquist *(11)*, which has become the standard for reporting Hg isotope data, is based on the scaling factors for kinetic mass-dependent fractionation and we suggest that those should be used in all subsequent studies to assure consistency of the data.

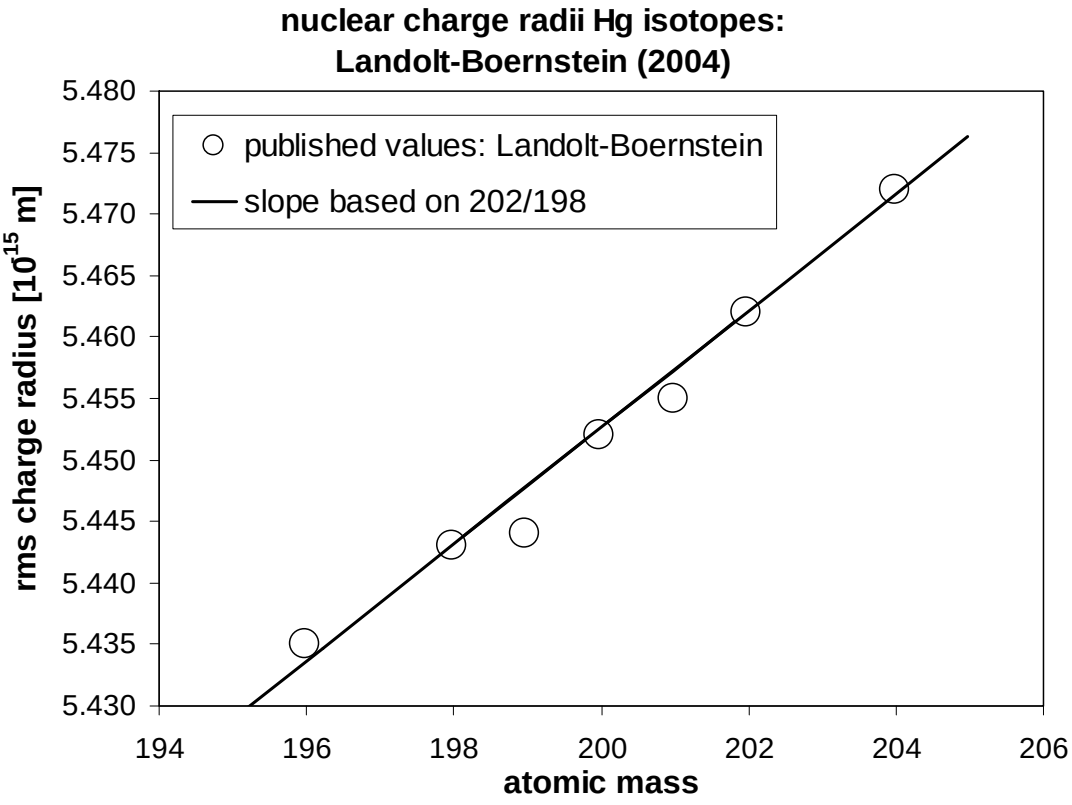

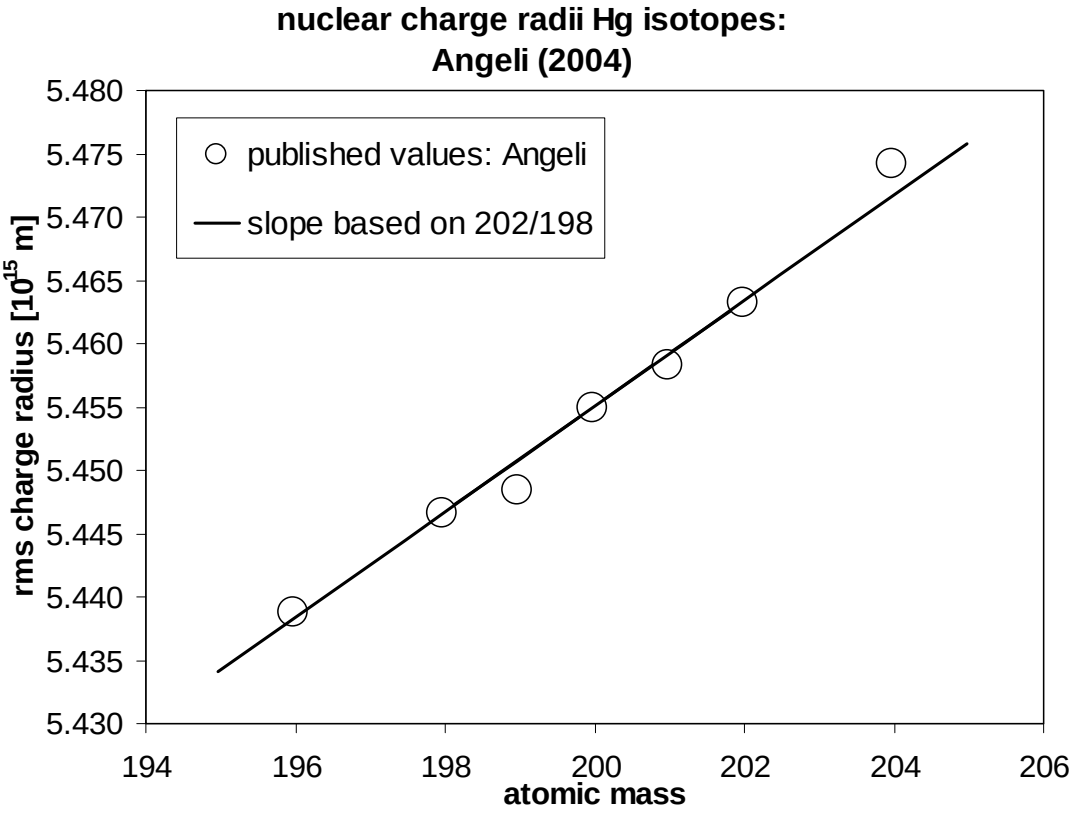

Figure S7: Comparison of nuclear charge radii by Landolt-Boernstein *(38)* and Angeli *(49)*